Septal Flash Assessment on CRT Candidates Based on Statistical Atlases of Motion

Nicolas Duchateau[1,2], Mathieu De Craene[1,2], Etel Silva[3], Marta Sitges[3], Bart H. Bijnens[1,2,4], and Alejandro F. Frangi[1,2,4]

[1] CISTIB - Universitat Pompeu Fabra, Barcelona, Spain
[2] CIBER-BBN, Spain
[3] Hospital Clinic - IDIBAPS - University of Barcelona, Spain
[4] ICREA, Barcelona, Spain

Abstract. In this paper, we propose a complete framework for the automatic detection and quantification of abnormal heart motion patterns using Statistical Atlases of Motion built from healthy populations. The method is illustrated on CRT patients with identified cardiac dyssynchrony and abnormal septal motion on 2D ultrasound (US) sequences. The use of the 2D US modality guarantees that the temporal resolution of the image sequences is high enough to work under a small displacements hypothesis. Under this assumption, the computed displacement fields can be directly considered as cardiac velocities. Comparison of subjects acquired with different spatiotemporal resolutions implies the reorientation and temporal normalization of velocity fields in a common space of coordinates. Statistics are then performed on the reoriented vector fields. Results show the ability of the method to correctly detect abnormal motion patterns and quantify their distance to normality. The use of local p-values for quantifying abnormal motion patterns is believed to be a promising strategy for computing new markers of cardiac dyssynchrony for better characterizing CRT candidates.

1 Introduction

Cardiac Resynchronization Therapy (CRT) has been shown to efficiently restore the coordination and relaxation among cardiac chambers, leading to better survival in patients with advanced heart failure and evidence of ventricular conduction delays [1]. The main clinical challenge for CRT is currently the understanding of physiological mechanisms involved behind positive or negative response. Recently, a promising way of finding non-responders for CRT was presented in [2], who proposed a classification of patients into classes of dyssynchrony patterns, and evaluated the response of each of these groups. This analysis attempts to relate the patient to a population with a known electrical or mechanical dyssynchrony defect that is expected to be effectively corrected by CRT. In this perspective, the computation of distances from a new subject to well identified groups of patients is a novel strategy for improving CRT response rate.

Recent research in computational anatomy has lead to the design and evaluation of statistical tools that synthesize the average anatomy within a population

G.-Z. Yang et al. (Eds.): MICCAI 2009, Part II, LNCS 5762, pp. 759–766, 2009.
© Springer-Verlag Berlin Heidelberg 2009

as well as the statistical deviation from this average. Recent works used non-rigid registration techniques to build Statistical Atlases of Motion of the heart from magnetic resonance image sequences [3], in which the displacement fields reflect the movement of anatomical structures. The use of 4D transformation models was presented in [4] for motion tracking over sequences of images. Registration is performed between frames at time points t_i and t_0 ($i \neq 0$). Such a strategy can provide large displacements, which in an atlas perspective would require to perform statistics on the tangent space of diffeomorphisms, using the methods described in [5]. In addition, representing the motion in reference to the first frame does not take advantage of the strong correlation between consecutive frames, and introduces a lot of redundancy between time steps for statistical computations.

A diffeomorphic registration scheme using paths between pairs of consecutive frames was recently presented in [6] for the synchronization of 4D time-series of cardiac images, and allows spatially consistent comparison of the supposedly temporally aligned sequences. One drawback of this technique is the fact that the computed transformations are only available at the discrete timepoints where the frames of the sequences are defined. Combining pairwise matching terms with the computation of diffeomorphic paths [7] allows to follow the evolution of a shape over a 2D+t sequence, and therefore to track the anatomy over the continuous timescale. However, this method still needs spatio-temporal synchronization steps to apply it for atlas construction from various sequences, and needs to prove its feasability when applied to real ultrasound (US) data.

In this paper we propose a complete and flexible pipeline for the construction of atlases of motion from sequences of US images, and illustrate its use for clinically-oriented quantitative comparison. We take advantage of registration between pairs of consecutive frames to work under a small displacements hypothesis. Our strategy is motivated by the fact that low correlation exists between time-distant frames for the US modality, and by the good temporal resolution of the 2D US modality. While existing atlases of motion are based on displacement fields, we prefer velocities, directly related to cardiac function. Working with small displacements allows easier definition of velocities over the whole continuous timescale, and direct computation of classical statistics on these velocities, once they have been brought to the same spatio-temporal system of coordinates. The structure provided by the atlas is then used for chosen pathology comparison to a healthy population, in the context of looking for CRT responders. We apply the method to the characterization of one mechanism related to Left Ventricle (LV) dyssynchrony, namely Septal Flash (SF), a quick inward/outward movement of the septum with respect to the LV, which occurs during the electrical activation of the heart chambers. We chose to work with 2D+t US modality as it is the only one used in clinical practice with sufficient temporal resolution to accurately identify fast septal motion patterns. However, the concepts developed in this paper could readily be applied to 3D+t once the required temporal resolution is accessible in standard clinical acquisition protocols.

2 Computation of Cardiac Velocities

2.1 Intra-sequence Registration

In the following we will denote $S = \{S(t_1), ..., S(t_i), ..., S(t_N)\}$ the temporal series of 2D images for one given patient,which contains N images taken at time-points t_i. To track the anatomy along cardiac cycles, pairwise registration between consecutive frames provides an optimal sequence of transformations $\boldsymbol{\varphi}_{t_i,t_{i+1}} : \boldsymbol{x} \mapsto \boldsymbol{x}'$ for each series, which map any point of image $S(t_i, \boldsymbol{x})$ to its corresponding point in the following frame $S(t_{i+1}, \boldsymbol{x}')$. Our non-rigid registration uses the Free-Form Deformation (FFD) method [8], which is made multi-resolution to improve its robustness to the position and spacing of control points. We used spacings of successively 26, 13 and 6.5 mm, and mutual information as matching term.

2.2 Small Displacements Hypothesis and Definition of Velocities

If the displacements are small, the logarithm [5] of a transformation $\log\left(\boldsymbol{\varphi}_{t_i,t_{i+1}}\right)$ can be approximated at the first order by its corresponding displacement field $\boldsymbol{\varphi}_{t_i,t_{i+1}} - \boldsymbol{Id}$. Velocities are directly obtained at the discrete time-points where the data is defined using

$$\forall i \quad (t_{i+1} - t_i) \cdot \boldsymbol{v}(t_i, .) = \log\left(\boldsymbol{\varphi}_{t_i,t_{i+1}}\right) \approx \left(\boldsymbol{\varphi}_{t_i,t_{i+1}} - \boldsymbol{Id}\right) \tag{1}$$

and assumed to be stationary between consecutive time-points t_i and t_{i+1}, which means that:

$$\boldsymbol{v}(t, \widehat{\boldsymbol{\varphi}}_{t_i,t}(\boldsymbol{x})) = \boldsymbol{v}(t_i, \boldsymbol{x}) \tag{2}$$

where t_i is the closest time-point that precedes t at which the series S is defined. Equation 2 means that trajectories are linearly interpolated to provide $\widehat{\boldsymbol{\varphi}}_{t_i,t}(\boldsymbol{x})$, the position at time t of the anatomical point that was at $\boldsymbol{x}$ at time t_i. Orientation and invertibility are preserved at any point $(t, \boldsymbol{x})$, as the log-exponential does with large displacements.

In our $t_i \rightarrow t_{i+1}$ registration approach, we can reasonably assume that the displacements are small. Such a choice is encouraged by the good temporal resolution of the 2D US modality. We validated this assumption by comparing the computed displacement fields and the logarithm of their relative transformations, using $D(\boldsymbol{\varphi_1}, \boldsymbol{\varphi_2}) = \frac{1}{card(\boldsymbol{\Omega})} \cdot \sum_{\boldsymbol{x_j} \in \boldsymbol{\Omega}} \frac{|\boldsymbol{\varphi_2} \circ \boldsymbol{\varphi_1}^{-1} - \boldsymbol{Id}|}{|\boldsymbol{\varphi_1} - \boldsymbol{Id}|}(\boldsymbol{x_j})$ as normalized dissimilarity measure between two transformations $\boldsymbol{\varphi_1}$ and $\boldsymbol{\varphi_2}$, where $\boldsymbol{\Omega}$ is the image domain. We previoulsy ensured these transformations are diffeomorphic, that-is-to-say they are invertible, smooth and with smooth inverse so that the logarithm can be computed. The results of this experiment are summarized in Fig.1, which presents the comparison of $\boldsymbol{\varphi}$ and $\log \boldsymbol{\varphi} + \boldsymbol{Id}$ for all the frames of one series containing three cycles. To get a range of comparison, this experiment is also done for a $0 \rightarrow t_i$ registration strategy, which works with larger displacements, and for a SF patient.

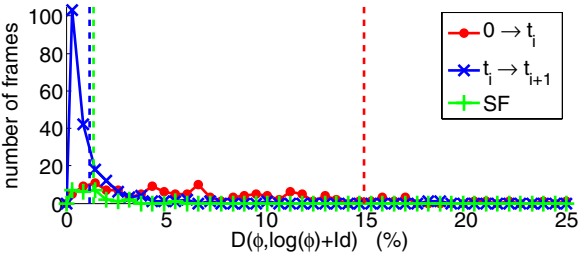

Healthy:	D_{small}	D_{acc}	(%)
$t_i \rightarrow t_{i+1}$	1.16	0.09	
$0 \rightarrow t_i$	14.87	0.42	
SF:			(%)
$t_i \rightarrow t_{i+1}$	1.35	0.03	

$D_{small}=D(\boldsymbol{\varphi},\log \boldsymbol{\varphi}+\boldsymbol{Id})$
$D_{acc}=D(\boldsymbol{\varphi},\exp(\log \boldsymbol{\varphi}))$

Fig. 1. Left: distribution of the dissimilarity measure D_{small} over the set of frames (*red* and *blue*: healthy volunteer, all the frames, $t_i \rightarrow t_{i+1}$ and $0 \rightarrow t_i$ approaches, *green*: SF patient, frames where SF occurs). Average over all the frames is in dashed line, and summed up in the table on the right. Table also contains D_{acc} for the assessment of logarithm computations accuracy.

2.3 Drift Correction

Drift artifacts from registration between pairs of consecutive frames are solved by applying for each cycle a correction involving a linear-in-time scaling of the transformation between frames which begin consecutive cycles, $\boldsymbol{\varphi}_{T_j,T_{j+1}}$, where T_j is the time-point starting cycle j. This transformation aims at correcting probe motion during the acquisition, and adds robustness towards out-of-plane motion, as the assumption $\boldsymbol{\varphi}_{T_j,T_{j+1}} = \boldsymbol{Id}$ generally made in other works [4] is not verified in our database of 2D US sequences.

3 Statistics on Cardiac Velocities

3.1 Pre-processing Steps

For each patient, the registration steps provide velocities on which statistics can be computed directly. They should first be brought into the same system of spatio-temporal coordinates. In the following we use k index to refer to sample patient k, and we index variable names accordingly.

Temporal Normalization. On each sequence, two control points related to the cardiac cycle phases are identified on the corresponding Electrocardiogram (ECG) and then mapped to a normalized timescale: the onset of QRS complex, using ECG tools from GE EchoPac software, and aortic valve closure, observed in left-parasternal long-axis images and located on ECG for the apical 4-chamber view we use by ECG correspondence. This step will be automated in further work. Between the control points temporal data is then adjusted linearly to match the new timescale. Similar synchronization methods [9] also identified a set of control points over each sequence of MR images, but used image similarity. We preferred to rely on ECG information, as for US images the identification of these points using image data can be biased by respiratory or probe motion. In addition, the use of physiological events as temporal landmarks is believed to be more extendable to handle pathological subjects.

Spatial Reorientation. Velocities $\boldsymbol{v}^k(t,\boldsymbol{x})$ are initially defined in the system of coordinates of patient k, but should be reoriented to be embedded in a reference system of coordinates before computing any statistics. We chose arbitrarily one series with good image quality as the reference. We first compute the transformation $\boldsymbol{\phi}^{k\rightarrow ref}(t,\boldsymbol{x})$ which maps estimated images of patient k and reference ref at time t, using FFD. We ensured that the computed transformation is invertible by checking that its jacobian has a positive determinant. Using notations of Section 2.2, an image S is simply estimated at time t from the image at the closest preceding time-point t_i, with $\widehat{S}(t,.) = \widehat{\boldsymbol{\varphi}}_{t_i,t}(S(t_i,.))$. Reorientation of velocity fields $\boldsymbol{v}^k$ is then achieved at every point $(t,\boldsymbol{x})$ using a push-forward action on vector fields [10]:

$$\mathcal{P}_\phi(\boldsymbol{v}) = \mathbf{D}\boldsymbol{\phi}\cdot\left(\boldsymbol{v}\circ\boldsymbol{\phi}^{-1}\right) \tag{3}$$

where $\boldsymbol{v} = \boldsymbol{v}^k$, $\boldsymbol{\phi} = \boldsymbol{\phi}^{k\rightarrow ref}$ and $\mathbf{D}$ the jacobian operator. We use the same computations for the inverse as in [5].

3.2 Statistical Computations

Once these pre-processing steps have been achieved, statistics can be directly computed on velocities. We first compute their average and variance to characterize the atlas population. Considering K different sample series $\left\{S^k|\ k = 1...K\right\}$, we obtain at any desired point $(t,\boldsymbol{x})$ the average $\overline{\boldsymbol{v}} = \frac{1}{K}\sum_{k=1}^{K}\boldsymbol{v}^k$ and the covariance matrix $\boldsymbol{\Sigma_v} = \frac{1}{K-1}\mathbf{V}^t\cdot\mathbf{V}$ from the set of velocities $\boldsymbol{v}^k$. Here $\mathbf{V}^t = \left[(\boldsymbol{v}^1-\overline{\boldsymbol{v}})|...|(\boldsymbol{v}^K-\overline{\boldsymbol{v}})\right]$ is the $2\times K$ matrix whose columns are the centered velocity samples at $(t,\boldsymbol{x})$, and ^{t} is the matrix transposition operator.

The atlas is then used for the comparison of the velocities of a given patient to the population used for its construction, through the computation at every desired point $(t,\boldsymbol{x})$ of statistical indexes assessing abnormality. We chose as index the p-value obtained from Hotelling's t-square statistic [11]:

$$t^2 = \alpha\ (\boldsymbol{v}-\overline{\boldsymbol{v}})^t\cdot\boldsymbol{\Sigma_v}^{-1}\cdot(\boldsymbol{v}-\overline{\boldsymbol{v}})$$

where $\alpha = K/(K+1)$, $\boldsymbol{v}$ is the velocity to compare to the atlas, and $\overline{\boldsymbol{v}}$ and $\boldsymbol{\Sigma_v}$ are the average and the covariance matrix computed for the population atlas.

	Healthy			SF		
(pixels)	δ_{inter}	δ_{intra}	Δ_{track}	δ_{inter}	δ_{intra}	Δ_{track}
1. Basal inferoseptal	2.21	1.90	1.57	1.29	2.43	1.73
2. Mid inferoseptal	2.51	3.58	3.84	0.41	1.84	1.26
3. Apical septal	1.66	3.97	5.11	0.70	2.03	2.67
4. Apical	0.97	2.17	2.76	0.77	2.72	1.67
Average	1.84	2.91	3.32	0.79	2.26	1.83

Fig. 2. Comparison between automatic and manual tracking: inter- and intra-operator standard deviation (δ_{inter} and δ_{intra}), and distance between automatically and manually tracked points (Δ_{track}).

4 Experiments on 2D US Sequences

We acquired 2D+t echocardiographic sequences in an apical 4-chamber view for two populations of patients, using a GE Vivid 7 machine. The atlas population was made up of 21 healthy volunteers. The second population included 4 CRT patients with visually assessed SF. The choice of the apical 4-chamber view is lead by the fact that it is the one used in clinical routine for the assessment of the inward/outward movement of the septum related to SF. Physiological differences between patients constrain the acquisition parameters, that will differ in terms of temporal resolution and image quality. For the atlas population, we acquired images with optimized resolution, that corresponds in average to a frame rate of 60 frames/s and a pixel size of 0.15×0.15 mm^2. For constraints related to the therapy, such settings were not reproducible for SF patients, acquired at a similar spatial resolution but at a lower frame rate (30 frames/s).

4.1 Atlas Construction

We first evaluated the quality of our intra-sequence registration by comparing it to manual landmarking. Three observers tracked 4 points along the septum that correspond to basal-inferoseptal, mid-inferoseptal, apical-septal and apical levels. Measurements were repeated 10 times for each point, and selection was done over one cycle of one healthy volunteer and one SF patient. Then each landmark was automatically tracked, starting from its average position in the first frame. Fig.2 presents the average in time of inter- and intra- observer variability, and compares it to the distance between automatically and manually tracked points. Automatic and manual tracking show comparable precision over all the selected points.

In order to check the efficiency of the synchronization scheme described in Section 3.1, we acquired 4 sequences for the same patient and checked that the

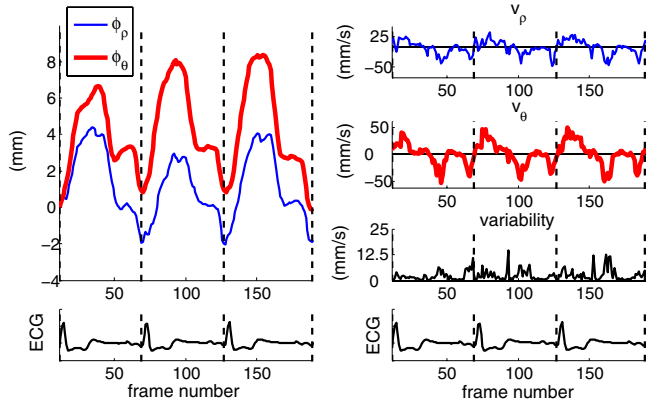

Fig. 3. Repeatability measurement for the spatio-temporal synchronization scheme. Left: radial (*thin blue*) and longitudinal (*thick red*) position of a tracked point at mid-inferoseptal level. Right: corresponding velocities. $\sqrt{Tr(\boldsymbol{\Sigma_v})}$ is used as variability measure.

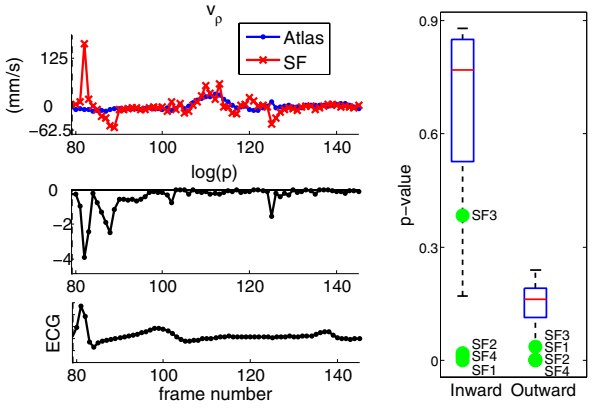

($\times 10^{-2}$)	Inward	Outward
SF1	$5.90e^{-3}$	0.20
SF2	1.89	0.12
SF3	38.37	3.68
SF4	1.09	0.02
Healthy	64.8	14.6

Fig. 4. Comparison of SF patients to the atlas, at mid-inferoseptal level. Left: radial velocity (*blue*: atlas average, *red*: SF1), and p-value plot along 1 cycle for SF1. Middle: p-value for the atlas population (*box plots*), and the 4 SF patients (*green dots*) at time-points corresponding to maximum inward (left) and outward (right) patterns. Right: table summarizing these p-values for the atlas (average of the leave-one-out values) and the 4 SF patients.

estimated velocities overlap after the synchronization. These sequences contain 3 whole cycles, and are made of 204, 189, 209 and 218 frames, respectively, with varying orientation of the probe. Good repeatability is observed between the curves, using $\sqrt{Tr(\boldsymbol{\Sigma_v})}$ as variability measure (Fig.3).

4.2 Septal Flash Assessment

We built the atlas of motion using the whole set of synchronized healthy volunteers, and then compared velocity fields for the atlas and the 4 SF patients as described in Section 3.2. The comparison is shown at mid-inferoseptal level, where the fast inward/outward motion of the septum takes place (Fig.4). Velocity and p-value profiles are plotted for one SF patient to see when SF occurs relatively to the ECG. Low p-value means high degree of abnormality. From both plots we can notice a very large abnormal inward velocity when the septum is activated, which is almost immediately followed by a fast outward motion at the time when the infero-lateral wall contracts. Box plots in the middle and the recapitulative table on the right compare p-values for the 4 SF patients and p-values for the atlas population, which were obtained using leave-one-out cross-validation. On SF patient 3 abnormality is hard to assess, due to the poor image quality of the sequence and the limited magnitude of the SF. On all the other three SF patients, p-value enables efficient assessment of abnormality for the SF pattern.

5 Conclusion

In this paper, we proposed to apply atlas quantification techniques to characterize the septal flash mechanism, which proved its interest for understanding

response to CRT. We proposed a complete framework for the construction of an atlas that represents motion in a standard spatio-temporal system of coordinates and compared cardiac velocities between CRT patients and a population of healthy subjects. Our experimental results demonstrated the ability of the atlas to assess local motion abnormalities in time and space. Our pipeline could easily be extended to strain measurements for a more advanced characterization of the mechanisms conditioning response to CRT.

Acknowledgments. This research has been partially funded by the Industrial and Technological Development Center (CDTI) under the CENIT Programme (CDTEAM Project) and the European Community's Seventh Framework Programme (FP7/2007-2013) under grant agreement n. 224495 (euHeart project).

References

1. Mullens, W., Grimm, R.A., Verga, T., Dresing, T., Starling, R.C., Wilkoff, B.L., Wilson Tang, W.H.: Insights From a Cardiac Resynchronization Optimization Clinic as Part of a Heart Failure Disease Management Program. J. Am. Coll. of Cardiology 53(9), 765–773 (2009)
2. Parsai, C., Bijnens, B.H., Sutherland, G.R., Baltabaeva, A., Claus, P., Marciniak, M., Paul, V., Scheffer, M., Donal, E., Derumeaux, G., Anderson, L.: Toward understanding response to cardiac resynchronization therapy: left ventricular dyssynchrony is only one of multiple mechanisms. Eur. Heart J. 30(8), 940–949 (2009)
3. Petitjean, C., Rougon, N., Cluzel, P., Prêteux, F., Grenier, P.: Quantification of myocardial function using tagged-MR and cine-MR images. Int. J. of Card. Im. 20(6), 497–508 (2004)
4. Ledesma-Carbayo, M.J., Kybic, J., Desco, M., Santos, A., Sühling, M., Hunziker, P.R., Unser, M.: Spatio-temporal nonrigid registration for ultrasound cardiac motion estimation. IEEE Trans. Med. Im. 24(9), 1113–1126 (2005)
5. Arsigny, V., Commowick, O., Pennec, X., Ayache, N.: A log-euclidean framework for statistics on diffeomorphisms. In: Larsen, R., Nielsen, M., Sporring, J. (eds.) MICCAI 2006. LNCS, vol. 4190, pp. 924–931. Springer, Heidelberg (2006)
6. Peyrat, J.-M., Delingette, H., Sermesant, M., Pennec, X., Xu, C., Ayache, N.: Registration of 4D time-series of cardiac images with multichannel diffeomorphic demons. In: Metaxas, D., Axel, L., Fichtinger, G., Székely, G. (eds.) MICCAI 2008, Part II. LNCS, vol. 5242, pp. 972–979. Springer, Heidelberg (2008)
7. Khan, A.R., Beg, M.F.: Representation of time-varying shapes in the large deformation diffeomorphic framework. In: ISBI, pp. 1521–1524 (2008)
8. Rueckert, D., Sonoda, L.I., Hayes, C., Hill, D.L., Leach, M.O., Hawkes, D.J.: Non-rigid registration using free-form deformations: application to breast MR images. IEEE Trans. Med. Im. 18(8), 712–721 (1999)
9. Perperidis, D., Mohiaddin, R.H., Rueckert, D.: Spatio-temporal free-form registration of cardiac MR image sequences. Med. Im. An. 9(5), 441–456 (2005)
10. Tu, L.W.: An Introduction to Manifolds, 1st edn., ch. 14. Springer, Heidelberg (2007)
11. Hotelling, H.: The Generalization of Student's Ratio. The Annals of Mathematical Statistics 2(3), 360–378 (1931)